ACS Photonics

Letter

pubs.acs.org/journal/apchd5

Label-Free Single Exosome Detection Using Frequency-Locked Microtoroid Optical Resonators

Judith Su*

Division of Biology and Biological Engineering, California Institute of Technology, Pasadena, California 91125, United States

Supporting Information

ABSTRACT: Recently exosomes have attracted interest due to their potential as cancer biomarkers. We report the real-time, label-free sensing of single exosomes in serum using microtoroid optical resonators. We use this approach to assay the progression of tumors implanted in mice by specifically detecting low concentrations of tumor-derived exosomes. Our approach measures the adsorption of individual exosomes onto a functionalized silica microtoroid by tracking changes in resonant frequency of the microtoroid. When exosomes land on the microtoroid, they perturb its refractive index in the evanescent field and thus shift its resonance frequency. Through digital frequency locking, we are able to rapidly track these shifts with accuracies of better than 10 attometers (one part in 10^{11}). Samples taken from tumor-implanted mice from later weeks generated larger frequency shifts than those from earlier weeks. Analysis of these shifts shows a distribution of unitary steps, with the maximum step having a height of ∼1.2 fm, corresponding to an exosome size of 44 ± 4.8 nm. Our results demonstrate the development of a minimally invasive tumor "biopsy" that eliminates the need to find and access a tumor.

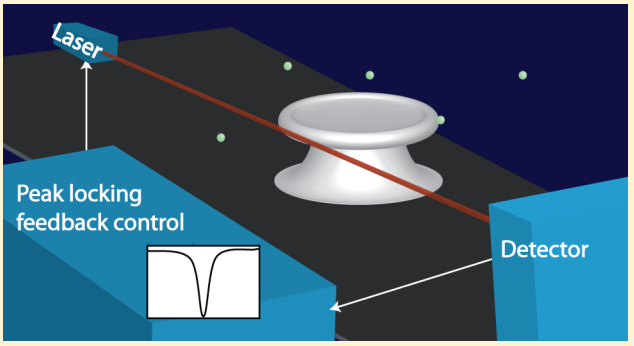

KEYWORDS: *label-free, exosome, microtoroid, optical resonator, biosensing, liquid biopsy*

Exosomes are small (∼30−100 nm) vesicles[1] that are shed by tumor cells into the bloodstream and, as such, are potential cancer biomarkers and intercellular communicators.[2−4] Noncancerous blood serum samples analyzed via nanoparticle tracking analysis (NTA) have been shown to contain a large number of exosomes, with one report indicating 3×10^6 exosomes per microliter[2] and another indicating 10^9 exosomes per microliter.[5] Rapid detection and quantification of low concentrations of exosomes can enable early detection of disease and provide information about its progression.[6] Fluorescent techniques such as stimulated emission depletion microscopy (STED)[7] and photoactivated localization microscopy (PALM)[8] have sensitivity to fluorophores at very low concentrations; however, labels are inconvenient, are not always possible to obtain for a particular application, are costly, and can introduce artifacts and limitations due to bleaching and blinking.[9,10] Current label-free sensing techniques such as nanoparticle tracking analysis[11] rely on the statistical analysis of large numbers of particles for particle detection and sizing (typical concentrations on the order of 10^{10} particles/mL).[12,13] Photonic crystals have been shown to detect bovine serum albumin at 10^{-13} M concentrations.[14] Differential heterodyne detection has been shown capable of detecting individual viruses.[15] Other label-free techniques such as lens-free holographic microscopy[16,17] can detect individual 40 nm particles, but not in solution.

Due to their small size and refractive index close to that of water, individual exosomes are challenging to detect in aqueous solution.[1] Recently fluid-filled nanomechanical cantilevers have been used to detect exosomes through changes in mass; however their lower detection limit in terms of number of exosomes is on the order of 10 000 exosomes.[18] In addition, a technique based on surface plasmon resonance through a functionalized nanohole array (nPLEX)[19] was used to sense no fewer than ∼3000 exosomes.

We have recently developed a label-free biosensing system called frequency locking optical whispering evanescent resonator (FLOWER) (Figure 1) that can detect single molecules in real time.[20] FLOWER is based upon optical resonator technology. Optical resonators[21−23] such as microspheres[24] and microtoroids[25,26] have enhanced sensitivity over techniques such as surface plasmon resonance, as light orbits their circumference many (>100 000) times, each time interacting with the analyte molecule(s) and generating a measurable signal output. In FLOWER, light is evanescently coupled into a glass microtoroid optical resonator using an optical fiber (Figure 1a). This light totally internally reflects inside the rim of the microtoroid, generating an evanescent field. At the resonance frequency, light constructively interferes, causing light recirculation and signal amplification. FLOWER

Received: March 23, 2015
Published: June 29, 2015

DOI: 10.1021/acsphotonics.5b00142
ACS Photonics 2015, 2, 1241−1245

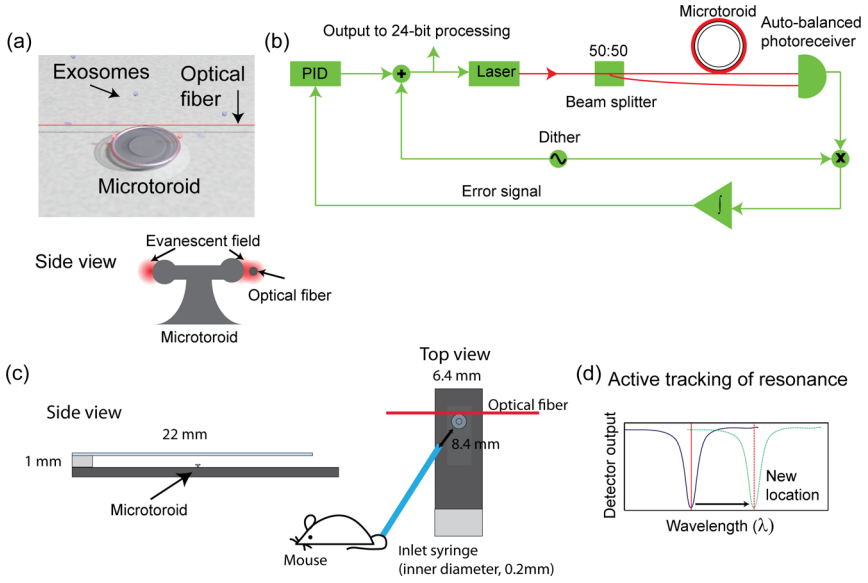

Figure 1. Overview of frequency locked optical whispering evanescent resonator (FLOWER). (a) Rendering of a microtoroid with light being evanescently coupled into it via an optical fiber. Particles bind to the rim of the microtoroid. (b) Block diagram of the sensing control system. A small high-frequency dither is used to modulate the driving laser frequency. When multiplied by the toroid output and time-averaged, this dither signal generates an error signal whose amplitude is proportional to the difference between the current laser frequency and resonance frequency. This error signal is sent to a proportional-integral-derivative (PID) controller whose output is used to set the laser frequency, thus completing the feedback loop. A computer records the observed frequency shifts. (c) Schematic of the sample cell from the side and top view. (d) We monitor changes in the resonance frequency of the microtoroid by monitoring dips in the transmitted intensity of the optical fiber (blue trace) as particles bind. This dip in the intensity of the optical fiber occurs when the frequency of light going through the fiber matches the resonance frequency of the microtoroid.

detects changes in the effective index of refraction (defined as the ratio of the index of refraction of the particle to the index of refraction of its surrounding media) of the microtoroid as particles enter its evanescent field. These index of refraction changes are detected by monitoring corresponding changes in the resonance frequency of the microtoroid.

What makes FLOWER different from other optical resonator biosensing platforms is that instead of continuously sweeping through a range of frequencies in order to locate the resonant frequency, FLOWER adaptively tracks the resonant frequency by locking the laser frequency onto the resonance of the microtoroid (Figure 1b,d). This adaptive locking lowers noise and also increases the sampling rate, thus permitting more computational filtering of the data. In this way FLOWER can more easily measure small discrete signal changes as particles bind. By relating measured signal changes to established theory,[24] FLOWER can make size, mass, and polarizability estimates of the bound exosome, thus providing further information regarding the parent tumor, without the need to find or access it.

RESULTS AND DISCUSSION

To test FLOWER's ability as an exosome sensor for medical diagnosis, athymic (nude) female mice (n = 5) born on the same day were implanted with Daudi (human Burkitt's lymphoma) tumor cells for 5 weeks. Five mice were chosen to determine whether a consistent correlation between the tumor progression and measurable signal levels existed. One microliter of serum from each mouse each week was diluted a million-fold in 0.9% saline and sequentially flowed over a microtoroid covalently functionalized with anti-CD81, an exosome-specific marker.[27] The sample cell (Figure 1c) was flushed two times with 0.9% saline, and the exosome-containing solution was introduced at a rate of 1 mL/min using a syringe pump. To minimize physical disturbances in the sample chamber, recordings were taken 30 s after the syringe pump had been stopped.

Resonance frequency changes in the microtoroid as particles bind were monitored using a photodetector by tracking dips in the optical transmission of the optical fiber used to couple light in the microtoroid. These transmission drops occur when the frequency of light in the fiber matches the resonance frequency of the microtoroid. The loaded quality factor Q of the microtoroids, which includes the perturbation loss resulting from the coupling fiber, ranged from 2×10^5–10^6 in solution.

Figure 2 shows recordings of the change in the resonance wavelength of the microtoroid over time as exosomes bind to

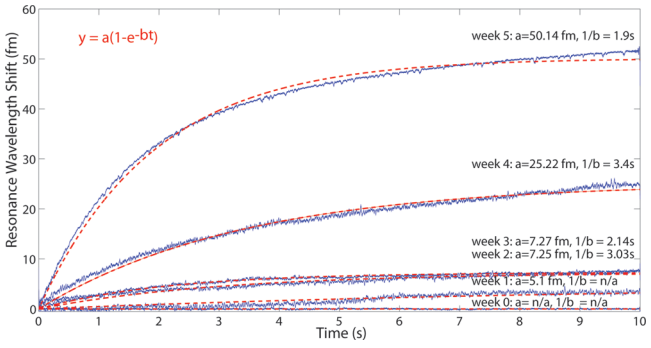

Figure 2. Exosome binding curves. Mice were implanted with human Burkitt's lymphoma tumor cells, and each week blood serum samples were taken and later analyzed all together using FLOWER. The curves shown here are from a single mouse. For each week we see an increase in the response from the sensor corresponding to increasing exosome levels. No significant signal was obtained from week 0. The data traces are fit with a simple exponential (dashed red line) corresponding to first-order kinetics.

DOI: 10.1021/acsphotonics.5b00142
ACS Photonics 2015, 2, 1241−1245

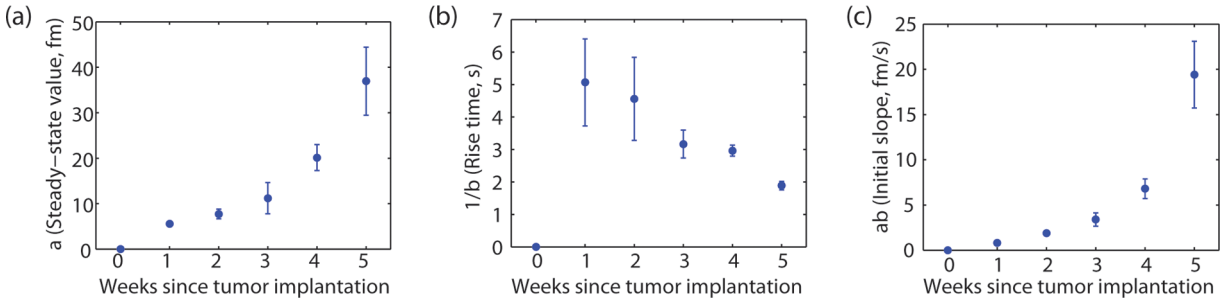

Figure 3. Compiled exosome detection results from all (n = 5) mice reflect tumor progression. (a) Fitted steady-state values increase monotonically, reflecting higher exosome concentrations at late stages. Center points represent the mean. Error bars represent the standard error of the mean. We note that data were collected for all mice for all weeks, with the exception of one mouse, for which data were collected only for weeks 0−2 due to the optical fiber breaking in the middle of the experiment. No blinding or randomization of samples was performed. (b) Rise times decrease monotonically, although the trend is not as pronounced as in (a). The value for week 0 is recorded as zero, as the trace was effectively flat. (c) Initial slope increases monotonically as more exosomes bind to the toroid per unit time.

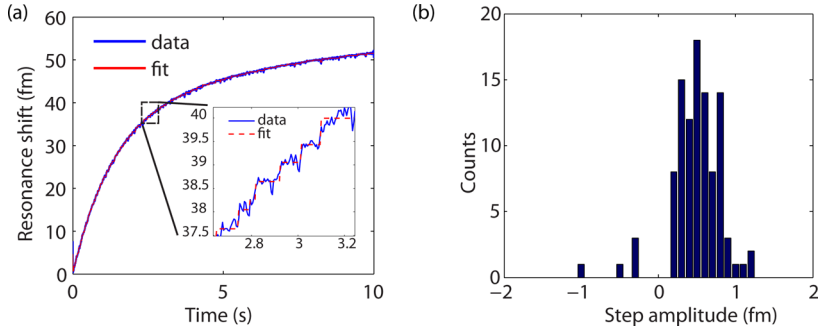

Figure 4. Toroid response data to a solution containing blood from a mouse with a tumor implanted in it for 5 weeks. (a) Zoom-in of week 5 and corresponding step-fit (red) and (b) histogram of step heights. Individual steps corresponding to the binding of individual exosomes may be seen. Negative step amplitudes represent step down or unbinding events.

its functionalized surface. Although no apparent binding occurred in response to the serum sample taken at week 0 at the time the tumor was implanted, samples from later weeks caused correspondingly greater shifts, indicating progression of the tumor. We can fit our binding curves to first order kinetics ($y = a(1-e^{-bt})$) (Figure 2).[28] As a result, the binding rate at any given time is proportional to the concentration of exosomes. Fit parameters are summarized for samples taken from each mouse in Figure 3a and b. At time t = 0, the binding rate given by the derivative (initial slope) of the binding curve is equal to the product (ab). Hence, this product (ab) can be used as a relative measure of exosome concentration and is plotted in Figure 3c. The steady-state value of the binding curve, plotted in Figure 3a, may also be used as a relative measure of concentration; however, the initial slope of the curve (Figure 3c is a better measure, as the standard deviation is smaller and the slope of the curve is steeper. This makes the initial slope curve more accurate at measuring smaller changes in concentration. Due to the complex flow conditions of the sample cell, absolute estimates of the exosome concentrations are difficult to obtain. This may be solved in future devices by flowing in a calibration solution of known concentration. A control experiment of a mouse without a tumor (SFigure 2) showed no relative increase in signal between samples taken from week 5 and week 1.

The ability to detect single exosomes as opposed to simply detecting overall concentration enables more sensitive and thus earlier detection of disease. Furthermore, being able to detect and characterize individual exosomes would provide some information regarding their cells of origin. A close inspection of a binding curve (week 5, Figure 4a, SFigure 3) shows discrete changes, or steps, in the resonance wavelength (λ) of the microtoroid. These wavelength steps occur because as a particle binds, the effective optical path length of the light within the microtoroid undergoes a sudden increase as light couples into the particle, causing the resonance wavelength of the microtoroid to shift to a new location. Subsequent binding events result in additional step shifts of the resonance wavelength of the microtoroid. The amplitude of each wavelength step shift depends on where on the resonator the particle lands. The maximum value of the step height ($\Delta\lambda$) (Figure 4b) for a given particle size occurs when that size of particle binds at the equator of the microtoroid where the electric field is greatest.[29] This maximum step height is shown in Figure 4b to be 1.2 fm and is directly related to particle size by[24]

$$d = 2a = 2\left(\frac{2V_m}{D}\frac{E_{0,max}^2}{E_0^2(r_s)}\right)^{1/3}\left(\frac{\Delta\lambda}{\lambda}\right)^{1/3} \quad (1)$$

where d is the diameter of a bound particle, a is the radius, V_m is the electromagnetic mode volume of the microtoroid, D is a dielectric factor calculated from the index of refraction of the bound particle and the background solution and found to be 0.5 (Supporting Information), $E_{0,max}^2$ is the electric field intensity at the microtoroid's equator, and $E_0^2(r_s)$ is the intensity of the electric field at the microtoroid's surface. V_m and $E_{0,max}^2/E_0^2(r_s)$ are determined from finite element simulations and were found to be 330 μm^3 and 5.5, respectively. We note that particles that bind to locations on the toroid's rim other than the equator will generate wavelength steps of smaller

DOI: 10.1021/acsphotonics.5b00142
ACS Photonics 2015, 2, 1241−1245

amplitude, as the electric field intensity is lower in those regions. These smaller step changes contribute to the overall width of the step amplitude histogram. Here, only the maximum step height corresponding to particles binding at the equator is used in extracting particle size information. A negative control of a binding experiment performed with a mismatched antibody (anti-TMV) showed no permanent binding steps (SFigure 4).

With the known refractive index of exosomes ($n = 1.375$)[30,31] we are able to calculate the size of the exosomes detected here as $d = 44 \pm 4.8$ nm, consistent with the expected size range for exosomes. Our error of ±4.8 nm was calculated on the basis of calibration experiments using ∼40 nm diameter polystyrene beads.[20] From this datum, we calculate a root-mean-square error of 16% ($n = 19$). As the polarizability of an exosome is different from a polystyrene bead, we state this as an estimate only.

This derived diameter of 44 nm agrees with the size range found from nanoparticle tracking analysis data for the same sample (SFigure 1). From the density (1.15 g/mL)[30] of an exosome, and assuming a spherical shape, this gives a mass of 57 ag or 3.4 MDa. The polarizability (α_{ex}) of the exosome is equal to Da^3 and may be calculated to be 6×10^{-24} m^3.[24]

CONCLUSION

Our work demonstrates the detection and tracking of the progression of a human tumor over time in a label-free fashion from a small volume of serum using a microtoroid optical resonator. We further demonstrate the label-free detection of single exosomes in serum and determine their size, mass, and polarizability. Such information provides insight into the tumor of origin without having to find or access the tumor. We anticipate that our results may provide the basis for a minimally invasive tumor biopsy and assist in early disease detection from a variety of samples.

METHODS

Microtoroid optical resonators were fabricated on a silicon chip according to conventional procedures.[26] The chip with the microtoroid was mounted on a stainless steel sample holder using double-sided tape. A sample chamber was created by epoxying a custom-cut coverslip to a microscope slide segment that was glued to the sample holder as a spacer (Figure 1c). Light was evanescently coupled into the microtoroid using an optical fiber that had been heated and thinned to allow for light to evanesce out and enter the microtoroid. A balanced detector was utilized to mitigate changes in signal (noise) due to power fluctuations of the laser. A tunable diode laser (center wavelength, 633 nm) was scanned in order to locate the resonance wavelength of the microtoroid. The resonance wavelength location of the toroid was deduced from a drop in the transmission of the optical fiber that occurs at resonance. The wavelength of the laser was then locked to the resonance wavelength of the microtoroid using a frequency-locking feedback controller (Toptica Photonics). The controller was locked at a dither frequency of 2 kHz, and the peak was tracked over a range of 632.5−637 nm. PID controller settings were set according to Ziegler−Nichols tuning rules. As particles bind to and change the resonant frequency of the microtoroid, the amount of voltage (which sets the wavelength) that the feedback controller applies to the tunable laser to stay locked to the resonance wavelength of the microtoroid is recorded (Figure 1). In this way particle-binding events are monitored.

Blood samples were spun down at 1200 rpm for 2 min. For selective particle binding, the microtoroids were functionalized with a custom-synthesized silane−PEG−maleimide linker. Mouse monoclonal anti-CD81 was bound to the maleimide. Prior to experiments, serum solutions were spun down in a Mini-Galaxy centrifuge and diluted 1 to 10^6 in 0.9% saline. Solutions from each week were thermally equilibrated for >1 h in a room-temperature water bath and then briefly vortexed for ∼2 s. Diluted samples were then sequentially flowed into the sample chamber at 1 mL/min using a syringe pump. Data recording began 30 s after the syringe pump was turned off. Particle binding "steps" were located via a step-finding algorithm.[32]

Computer code and raw data are archived and may be obtained through e-mail. Mouse monoclonal anti-CD81 was obtained from Santa Cruz Biotechnology (sc-7637). Experiments were approved by the California Institute of Technology Institutional Biosafety Committee.

ASSOCIATED CONTENT

Supporting Information

The Supporting Information is available free of charge on the ACS Publications website at DOI: 10.1021/acsphotonics.5b00142.

AUTHOR INFORMATION

Corresponding Author

*E-mail: judy@caltech.edu.

Notes

The authors declare no competing financial interest.

ACKNOWLEDGMENTS

We thank Andrew Raubitschek and Desiree Crow at the COH for the exosome samples and Scott Fraser (Caltech/USC) for discussions. This research was supported in part by the Caltech−UCLA Joint Center for Translational Medicine and a National Research Service Award (T32GM07616) from the National Institute of General Medical Sciences.

REFERENCES

(1) van der Pol, E.; Hoekstra, A. G.; Sturk, A.; Otto, C.; van Leeuwen, T. G.; Nieuwland, R. Optical and non-optical methods for detection and characterization of microparticles and exosomes. *J. Thromb. Haemostasis* **2010**, *8*, 2596−607.

(2) Vlassov, A. V.; Magdaleno, S.; Setterquist, R.; Conrad, R. Exosomes: current knowledge of their composition, biological functions, and diagnostic and therapeutic potentials. *Biochim. Biophys. Acta, Gen. Subj.* **2012**, *1820*, 940−8.

(3) Simpson, R. J.; Lim, J. W.; Moritz, R. L.; Mathivanan, S. Exosomes: proteomic insights and diagnostic potential. *Expert Rev. Proteomics* **2009**, *6*, 267−83.

(4) van der Pol, E.; van Gemert, M. J.; Sturk, A.; Nieuwland, R.; van Leeuwen, T. G. Single vs. swarm detection of microparticles and exosomes by flow cytometry. *J. Thromb. Haemostasis* **2012**, *10*, 919−30.

(5) Oksvold, M. P.; Kullmann, A.; Forfang, L.; Kierulf, B.; Li, M.; Brech, A.; Vlassov, A. V.; Smeland, E. B.; Neurauter, A.; Pedersen, K. W. Expression of B-Cell Surface Antigens in Subpopulations of Exosomes Released From B-Cell Lymphoma Cells. *Clin. Ther.* **2014**36, 847−862.e1.10.1016/j.clinthera.2014.05.010

DOI: 10.1021/acsphotonics.5b00142
ACS Photonics 2015, 2, 1241−1245

(6) van der Pol, E.; Boing, A. N.; Harrison, P.; Sturk, A.; Nieuwland, R. Classification, functions, and clinical relevance of extracellular vesicles. *Pharmacol. Rev.* **2012**, *64*, 676−705.
(7) Hell, S. W.; Wichmann, J. Breaking the diffraction resolution limit by stimulated emission: stimulated-emission-depletion fluorescence microscopy. *Opt. Lett.* **1994**, *19*, 780−2.
(8) Betzig, E.; Patterson, G. H.; Sougrat, R.; Lindwasser, O. W.; Olenych, S.; Bonifacino, J. S.; Davidson, M. W.; Lippincott-Schwartz, J.; Hess, H. F. Imaging intracellular fluorescent proteins at nanometer resolution. *Science* **2006**, *313*, 1642−5.
(9) Moerner, W. E. Those Blinking Single Molecules. *Science* **1997**, *277*, 1059−1060.
(10) Peterman, E. J.; Sosa, H.; Moerner, W. E. Single-molecule fluorescence spectroscopy and microscopy of biomolecular motors. *Annu. Rev. Phys. Chem.* **2004**, *55*, 79−96.
(11) Filipe, V.; Hawe, A.; Jiskoot, W. Critical evaluation of Nanoparticle Tracking Analysis (NTA) by NanoSight for the measurement of nanoparticles and protein aggregates. *Pharm. Res.* **2010**, *27*, 796−810.
(12) Roding, M.; Deschout, H.; Braeckmans, K.; Sarkka, A.; Rudemo, M. Self-calibrated concentration measurements of polydisperse nanoparticles. *J. Microsc.* **2013**, *252*, 79−88.
(13) van der Pol, E.; Coumans, F.; Varga, Z.; Krumrey, M.; Nieuwland, R. Innovation in detection of microparticles and exosomes. *J. Thromb. Haemostasis* **2013**, *11* (Suppl 1), 36−45.
(14) Baker, J. E.; Sriram, R.; Miller, B. L. Two-dimensional photonic crystals for sensitive microscale chemical and biochemical sensing. *Lab Chip* **2015**, *15*, 971−90.
(15) Mitra, A.; Deutsch, B.; Ignatovich, F.; Dykes, C.; Novotny, L. Nano-optofluidic Detection of Single Viruses and Nanoparticles. *ACS Nano* **2010**, *4*, 1305−1312.
(16) McLeod, E.; Dincer, T. U.; Veli, M.; Ertas, Y. N.; Nguyen, C.; Luo, W.; Greenbaum, A.; Feizi, A.; Ozcan, A. High-Throughput and Label-Free Single Nanoparticle Sizing Based on Time-Resolved On-Chip Microscopy. *ACS Nano* **2015**, *9*, 3265.
(17) McLeod, E.; Nguyen, C.; Huang, P.; Luo, W.; Veli, M.; Ozcan, A. Tunable vapor-condensed nanolenses. *ACS Nano* **2014**, *8*, 7340−9.
(18) Olcum, S.; Cermak, N.; Wasserman, S. C.; Christine, K. S.; Atsumi, H.; Payer, K. R.; Shen, W.; Lee, J.; Belcher, A. M.; Bhatia, S. N.; Manalis, S. R. Weighing nanoparticles in solution at the attogram scale. *Proc. Natl. Acad. Sci. U. S. A.* **2014**, *111*, 1310−5.
(19) Im, H.; Shao, H.; Park, Y. I.; Peterson, V. M.; Castro, C. M.; Weissleder, R.; Lee, H. Label-free detection and molecular profiling of exosomes with a nano-plasmonic sensor. *Nat. Biotechnol.* **2014**, *32*, 490−5.
(20) Su, J.; Goldberg, A. F. G.; Stoltz, B. Label-free detection of single nanoparticles and biological molecules using microtoroid optical resonators. *Light: Sci. Appl.* **2015**, in press.
(21) Fan, X.; White, I. M.; Shopova, S. I.; Zhu, H.; Suter, J. D.; Sun, Y. Sensitive optical biosensors for unlabeled targets: a review. *Anal. Chim. Acta* **2008**, *620*, 8−26.
(22) Kindt, J. T.; Bailey, R. C. Biomolecular analysis with microring resonators: applications in multiplexed diagnostics and interaction screening. *Curr. Opin. Chem. Biol.* **2013**, *17*, 818−26.
(23) Lin, S.; Crozier, K. B. Trapping-assisted sensing of particles and proteins using on-chip optical microcavities. *ACS Nano* **2013**, *7*, 1725−30.
(24) Arnold, S.; Khoshsima, M.; Teraoka, I.; Holler, S.; Vollmer, F. Shift of whispering-gallery modes in microspheres by protein adsorption. *Opt. Lett.* **2003**, *28*, 272−4.
(25) Vahala, K. J. Optical microcavities. *Nature* **2003**, *424*, 839−46.
(26) Armani, D. K.; Kippenberg, T. J.; Spillane, S. M.; Vahala, K. J. Ultra-high-Q toroid microcavity on a chip. *Nature* **2003**, *421*, 925−8.
(27) Masyuk, A. I.; Masyuk, T. V.; Larusso, N. F. Exosomes in the pathogenesis, diagnostics and therapeutics of liver diseases. *J. Hepatol.* **2013**, *59*, 621−5.
(28) Connors, K. A. *Chemical Kinetics: The Study of Reaction Rates in Solution*; VCH: New York, NY, 1990.
(29) Oxborrow, M. Traceable 2-D finite-element simulation of the whispering-gallery modes of axisymmetric electromagnetic resonators. *IEEE Trans. Microwave Theory Tech.* **2007**, *55*, 1209−1218.
(30) Miksa, M.; Wu, R.; Dong, W.; Komura, H.; Amin, D.; Ji, Y.; Wang, Z.; Wang, H.; Ravikumar, T. S.; Tracey, K. J.; Wang, P. Immature dendritic cell-derived exosomes rescue septic animals via milk fat globule epidermal growth factor-factor VIII [corrected]. *J. Immunol.* **2009**, *183*, 5983−90.
(31) van der Pol, E.; Coumans, F. A.; Sturk, A.; Nieuwland, R.; van Leeuwen, T. G. Refractive index determination of nanoparticles in suspension using nanoparticle tracking analysis. *Nano Lett.* **2014**, *14*, 6195−201.
(32) Kerssemakers, J. W.; Munteanu, E. L.; Laan, L.; Noetzel, T. L.; Janson, M. E.; Dogterom, M. Assembly dynamics of microtubules at molecular resolution. *Nature* **2006**, *442*, 709−12.

DOI: 10.1021/acsphotonics.5b00142
ACS Photonics 2015, 2, 1241−1245